



<http://www.diva-portal.org>

Postprint

This is the accepted version of a paper published in . This paper has been peer-reviewed but does not include the final publisher proof-corrections or journal pagination.

Citation for the original published paper (version of record):

Sun, D., Kiselev, A., Liao, Q., Stoyanov, T., Loutfi, A. (2020)
A New Mixed Reality - based Teleoperation System for Telepresence and
Maneuverability Enhancement
IEEE Transactions on Human-Machine Systems, 50(1): 55-67
<https://doi.org/10.1109/THMS.2019.2960676>

Access to the published version may require subscription.

N.B. When citing this work, cite the original published paper.

Permanent link to this version:

<http://urn.kb.se/resolve?urn=urn:nbn:se:oru:diva-77829>

A New Mixed Reality - Based Teleoperation System for Telepresence and Maneuverability Enhancement

Da Sun, Andrey Kiselev, Qianfang Liao, Todor Stoyanov and Amy Loutfi .

Abstract—Virtual Reality (VR) is regarded as a useful tool for teleoperation system that provides operators an immersive visual feedback on the robot and the environment. However, without any haptic feedback or physical constructions, VR-based teleoperation systems normally have poor maneuverability and may cause operational faults in some fine movements. In this paper, we employ Mixed Reality (MR), which combines real and virtual worlds, to develop a novel teleoperation system. New system design and control algorithms are proposed. For the system design, a MR interface is developed based on a virtual environment augmented with real-time data from the task space with a goal to enhance the operator's visual perception. To allow the operator to be freely decoupled from the control loop and offload the operator's burden, a new interaction proxy is proposed to control the robot. For the control algorithms, two control modes are introduced to improve long-distance movements and fine movements of the MR-based teleoperation. In addition, a set of fuzzy logic based methods are proposed to regulate the position, velocity and force of the robot in order to enhance the system maneuverability and deal with the potential operational faults. Barrier Lyapunov Function (BLF) and back-stepping methods are leveraged to design the control laws and simultaneously guarantee the system stability under state constraints. Experiments conducted using a 6-Degree of Freedom (DoF) robotic arm prove the feasibility of the system.

I. INTRODUCTION

Teleoperation allows human operators to perform unreachable or hazardous tasks at a remote distance. With this property, it is widely used in outer space exploration, underwater operation, nuclear reaction and minimally invasive surgery [1]. In recent years, teleoperation has been deeply explored on passivity/stability maintenance [2]–[5], transparency enhancement [6]–[8], haptic feedback [9]–[14] and disturbances compensation [15]–[17]. However, when it comes to the teleoperation control of industrial robots, the practical workspace and Degree of Freedom (DoF) of the master haptic device usually cannot cover those of the industrial robot, due to asymmetrical master-slave robotic mechanical structures. Moreover, in most of the teleoperation studies, visual feedback is seldom considered and human operator is assumed to have a full vision on the robot and the environment. In reality, even with ideal position and force tracking, a teleoperation system can hardly perform remote tasks without considering the visualization

issues of the environment and the robot, because operators still have difficulties in judging the objects' distances or identifying the right object to interact with [18]. In some studies, less complex methods utilize static cameras or monitors to provide a mono-vision feedback [19], [20]. Nevertheless, the human perception of distances is seriously constrained by the lack of stereoscopic vision and parallax to the extent that telepresence enhancement of those systems is still an open issue.

In order to reinforce human situational awareness on the real environment and simultaneously break the physical restriction on the master mechanism, Virtual Reality (VR) has long been advocated as a promising technology for teleoperation interfaces. However, popularization of VR technology has only been possible lately because of availability of consumer-grade interface hardware, such as gaming Head-Mounted Display (HMD), and increased computing power. Teleoperation applications usually utilize some sort of Mixed Reality (MR)-based interfaces because in one way or another they deal with physical objects and parts of physical and virtual worlds need to be mixed together. Because the exact way how real and virtual objects are blended may vary, the concept of reality-virtuality continuum and a variety of MR settings are introduced in [21]. The authors propose a method to describe a particular implementation of a MR system based on a three-dimensional taxonomy, which includes such factors, as Reality, Immersion, and Directness. This allows to account for a multitude of various aspects simultaneously. An interface based on Augmented Virtuality (AV) setting is introduced in [22] in order to improve performance in the pick-and-place task. Further, it also allows to bridge the gap in performance between experienced and novice operators. This result is in line with the previously discovered guidelines by [23], which highlights, among other factors, the importance of providing fused sensor data using a single display, which is achieved by using AV in combination with a HMD technology. The result is also supported by the study in application to mobile robot teleoperation by [24] which demonstrates that 3D interfaces can improve telepresence. In [25], operators' effectiveness is improved in Search-and-Rescue scenario by using a HMD with operator's head tracking, which provides both, stereoscopic vision and a parallax effect. In [26], a 3D scan of the scene is developed to generate a set of potential grasp candidates on the objects to provide guidance for teleoperation.

From the above references, MR-based teleoperation can provide higher telepresence and have larger potential on robot performance improvement over the traditional teleoperation in several respects. Firstly, it can provide the operator an immersive visual feedback about the remote environment. Secondly,

* This work has been funded by The Knowledge Foundation (www.kks.se) under the scope of the project AMICI: Augmented Interaction for Human-Robot Collaborative Tasks in Industrial Environments.

The authors are with the Center for Applied Autonomous Sensor Systems, Örebro University, Sweden. (corresponding author: Qianfang Liao)

E-mail addresses: Da.Sun@oru.se (D. Sun), Andrey.Kiselev@oru.se (A. Kiselev), Qianfang.Liao@oru.se (Q. Liao), Todor.Stoyanov@oru.se (T. Stoyanov), Amy.Loutfi@oru.se (A. Loutfi)

unlike the traditional bilateral teleoperation that struggles with the asymmetry between master and slave robots, the MR interface has no physical restriction on the robots' mechanism, the practical workspace, or the robot's DoF. Thus, the MR interface provides a larger freedom on teleoperation control. However, its intrinsic shortage, lacking any haptic feedback or physical construction, limits its use for precise control and increases the operational difficulty. How to enhance the system's maneuverability is a challenge.

This paper proposes a novel MR-based teleoperation system, where new system design and novel control algorithms are developed to enhance the telepresence and maneuverability. The contribution of this paper is as follows:

- For system design:
 - A new MR interface is designed to teleoperate an industrial robot with multiple DoF, in which an immersive HMD based interface is built with head and hand gestures tracking. The proposed MR interface provides immersive visual feedback to enhance the system's telepresence.
 - Inside the MR interface, an interaction proxy is designed to teleoperate the robot which allows richer and more natural human-environment interaction. Compared to previous teleoperation systems (e.g. [27], [28]) that have physical restrictions on the master controllers and are seriously affected by the human motion, the designed interaction proxy gives the operator larger freedoms and convenience to manipulate the robot. Thus, the system maneuverability can be enhanced.
- For control algorithms:
 - Two control modes are proposed to enhance long-distance movement and fine movement of the MR-based teleoperation system. The combination of the two control modes supports a smooth robot's motion.
 - Based on the two control modes, a series of fuzzy logic-based control algorithms are proposed to regulate the robot's position, velocity, and force and update its workspace in order to handle the potential operational faults and enhance the robot's maneuverability.
 - Barrier Lyapunov Function (BLF) and back-stepping methods are used to design the control laws and to guarantee stability of the MR-based teleoperation system under state constraints.

II. MR-BASED INTERFACE

The system architecture is presented in Fig. 1. The task space contains a multi-DoF industrial robot and RGB-D sensors. Robot Operating System (ROS) is used as a foundation framework for all units in the task space. Further, to allow better system flexibility, the robot and each sensor run their own ROS instances. This allows to introduce new sensors into the task space without the need to modify any other parts and also allows to use different versions of ROS, which is not possible in the master-slave setting.

The MR-based interface is established by virtue of Unity3D graphics framework. One main merit of the Unity3D graphics framework is minimization of the development effort in such areas as low-level graphics, display management (particularly,

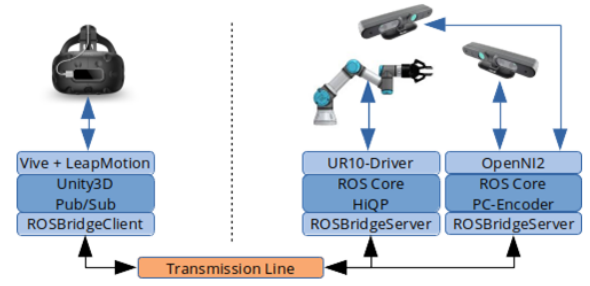


Figure 1. System architecture. The task space containing the robot and RGB-D sensor is connected to the MR-interface with a transmission line.

rendering for HMD), user interaction physics, and animation. However, it also introduces challenges in connecting the interface to the robot part. ROSBridge protocol is applied in this study to connect the MR-based interface to the robot, which provides a socket-based transport for ROS messages between a host system (the robot side) and any third-party software. Therefore, every unit in the task space implements ROSBridge server, to which the MR interface connects. The server-side ROSBridge package is further developed to implement binary data transfer and message compression to reduce the bandwidth. The interface side implements ROSBridge connector that is publishing a number of messages related to desired pose, the operator's pose in the environment, gestures, and status of UI elements.

The implemented interface applies an AV setting, where the scene contains a model of the robot in a virtual environment, augmented with real-time robot joint states and point cloud of the task space from a RGB-D sensor. The AV setting is selected to isolate an operator from their local environment and direct attention to the remote task space. Additionally, the interaction paradigm, described in further details in III, is build to allow third-person view of the scene, with an operator decoupled from the control loop. To reduce the bandwidth, the interface part is subscribed to a combined row imagery data from the sensor, transmitted at the rate of 10 frames per second. The point cloud reconstruction is then performed on the interface part. This allows to greatly reduce the bandwidth and also implement selective point cloud rendering on the interface side. The bandwidth between the robot and the interface side is 1.5MB/s, which includes all ROS messages and RGB-D sensor images.

III. FUZZY LOGIC BASED MR-TELEOPERATION

The main goal of developing the interface in this study is to allow the operator to interact with the environment in a natural way. Accordingly, a HMD is applied in order to allow the operator to move freely in the virtual task space and to provide stereoscopic vision and parallax effect. This is achieved by using HTC Vive HMD in a big-room setting (ca 3×4 meters). Further, the operator's hands are tracked using a Leap Motion gesture tracker mounted on the HMD. The benefit of this is that the operator can interact with the environment using hand gestures. Unlike previous works, the gesture captured by the Leap Motion sensor in this study is not directly used to

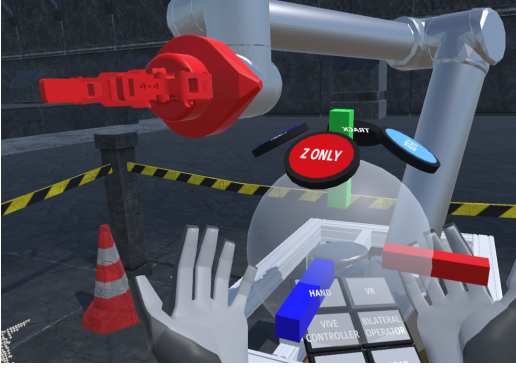


Figure 2. Interaction proxy in the virtual environment, which is the transparent sphere with a coordinate frame and some buttons. The coordinate frame is used for targeting the desired pose, and the virtual buttons, which can be freely attached to the interaction proxy, are linked to different functions

control the robot since it can easily generate tracking errors. Instead, an "interaction proxy" is designed in the MR-based interface to control the position and orientation of the robot in order to ease the operator's task. The interaction proxy is a virtual object, which can be freely rotated and moved by the operator inside the virtual environment as shown in Fig. 2. Compared with the VR controllers in [22] and [27] where the operator has to physically grasp a handle and cannot let go of it when controlling the robot, a salient advantage of the proposed virtual proxy is that the operator is not required to physically hold anything, and can be freely decoupled from the control loop at any moment to take a rest or change a pose to proceed with the next motion. Therefore, the burden of performing tasks on the operator can be alleviated, and the chance that the robot will be disturbed by unintentional operator's gestures can be reduced.

However, since the virtual proxy cannot be physically touched, it is easy for the operator to give operational faults. In order to solve this problem and enhance the system maneuverability, we propose two control modes (Coarse Movement Mode (CMM) and Fine Movement Mode (FMM)) together with a series of robot states regulation strategies. A virtual button is created at the interaction proxy that can switch between "activated" and "deactivated" through pressing it in the virtual environment, and we use this button to switch the two control modes. CMM is designed for the robot's long-distance movement. In this mode, at the beginning, the button is deactivated to lock the robot's motion and make it stay at its current pose so that the operator can freely adjust the position and orientation of the interaction proxy. After placing the interaction proxy in the desired location, the operator can activate the button by pressing it to allow the robot to track the interaction proxy. With this function, the robot does not need to continuously follow the virtual proxy in CMM, and the operator can have enough time to place the virtual proxy in the desired pose when the button is deactivated. As a result, operational faults can be basically avoided. On the other hand, FMM is designed for fine movement by providing the robot continuous references, where the button is always activated such that the interaction proxy continuously influence

the movement of the robot. To prevent the operational fault in FMM, effective strategies are needed to regulate the robot states including orientation, position and velocity. In the remainder of this section, the regulations of orientation, position, velocity and force in the two control modes are introduced.

A. Orientation regulation: As stated before, in CMM, by deactivating the button to lock the robot's motion, the operator can freely adjust the interaction proxy without influencing the robot. Therefore, the operator can have sufficient time to determine an appropriate orientation for the robot through the virtual proxy. In FMM where the robot continuously tracking the interaction proxy, the robot performing task will be a difficult work with heavy burden for the operator since s/he needs to simultaneously take care of both position and orientation for a multi-DoF robot. To solve this issue, at the moment that the button is activated (FMM is launched), the current reference orientation is recorded as ${}^oX_{str}$ and is taken as the reference orientation for FMM. Therefore, in FMM, the orientation reference is always constant as ${}^oX_{str}$ and the operator only needs to regulate the position of the robot. ${}^oX_{str}$ can be updated during CMM.

B. Position regulation: We firstly introduce the position regulation in FMM. A fuzzy logic-based method is applied to regulate the reference position signal as shown in Fig. 3, where X_{r1} represents the position of the center of the interaction proxy and X_{r3} denotes the current position of the end effector X_s . Two concentric spheres is designed with the center of the spheres located at the tip of the robot. Their radius are r and R , ($R > r$). The two spheres represent the workspaces of the robot in its current states. Then, build a straight line created by X_{r1} and X_{r3} . X_{r2} is the point of intersection between the line and the small sphere. (There are two points of intersection of the straight line and the small sphere, and the one closest to X_{r1} is the one we need.) The position error between the interaction proxy and the robot is defined as

$$e_p(t) = X_{r1}(t - T) - X_o(t) \quad (1)$$

where T denote the time delay. X_o denotes the recorded initial position of the robot. Based on $e_p(t)$, we define the fuzzy memberships μ_1 , μ_2 and μ_3 to be

$$\mu_1 = \begin{cases} 1 & \text{if } \|e_p\|_2 \leq r \\ \frac{1}{2}(\frac{R}{R-r} - \frac{1}{R-r} \|e_p\|_2)^\sigma + \frac{1}{2} & \text{if } r < \|e_p\|_2 \leq R \\ -\frac{1}{2}\tanh(\iota(\|e_p\|_2 - R)) + \frac{1}{2} & \text{if } \|e_p\|_2 > R \end{cases} \quad (2)$$

$$\mu_2 = \begin{cases} 0 & \text{if } \|e_p\|_2 \leq r \\ \frac{1}{2} - \frac{1}{2}(\frac{R}{R-r} - \frac{1}{R-r} \|e_p\|_2)^\sigma & \text{if } r < \|e_p\|_2 \leq R \\ -\frac{1}{2}\tanh(\iota(\|e_p\|_2 - R)) + \frac{1}{2} & \text{if } \|e_p\|_2 > R \end{cases} \quad (3)$$

$$\mu_3 = \begin{cases} 0 & \text{if } \|e_p\|_2 \leq R \\ \tanh(\iota(\|e_p\|_2 - R)) & \text{if } \|e_p\|_2 > R \end{cases} \quad (4)$$

where $\sigma > 1$ and $\iota \gg 1$ are positive constants, whose values determine the change rates. μ_1 , μ_2 and μ_3 satisfy $\mu_1 + \mu_2 + \mu_3 = 1$. Fig. 4 shows a example of the above fuzzy membership. The final reference position can be derived as

$$X_r(t) = \mu_1 X_{r1}(t - T) + \mu_2 X_{r2}(t) + \mu_3 X_{r3}(t) \quad (5)$$

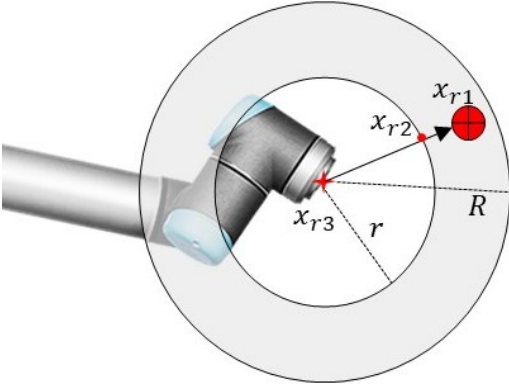
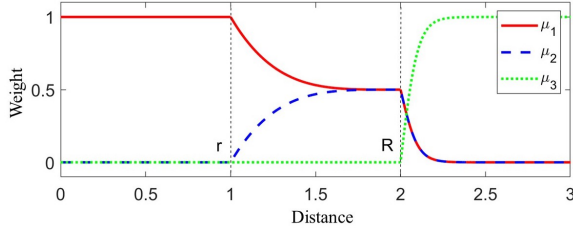


Figure 3. Definition of concentric circle workspace

Figure 4. Example diagram of μ_1, μ_2, μ_3 , ($r = 1, R = 2, \sigma = 4, \iota = 20$)

According to (2)-(5) and Fig. 4, when the interaction proxy is inside the small sphere ($\|e_p\|_2 < r$), it takes the full right to drive the robot. When it is between the small sphere and the large sphere ($r \leq \|e_p\|_2 \leq R$), the target pose of the robot is co-determined by X_{r2} and X_{r1} . By setting $\sigma > 1$, the control authority of X_{r1} can be fast transferred to X_{r1} and X_{r2} , so that the robot can be "dragged" by X_{r2} , and will not exceed the large workspace. When the interaction proxy is outside the large sphere ($\|e_p\|_2 > R$), this is defined as an operational fault. By setting $\iota \gg 1$, the robot is basically not controlled by the interaction proxy, and will stay at its current position along with μ_3 sharply increasing to 1.

The workspaces will then update, when the robot X_s reaches the reference position X_r (the tracking error e_s is small enough). That is, $(\|e_s\|_2 = \|X_s - X_r(t-T)\|_2)^2 \leq \xi_s^2$, where ξ_s is a positive constant close to zero. The initial position X_o also updates to be the current robot position when which updates when $\|X_s - X_r\|_2 \leq \xi_s$.

By leveraging the above fuzzy memberships and the update rules, the updating workspace allows the interaction proxy to drive the robot to make a small movement in every step time, in case that the sudden-jumped interaction proxy caused by operational faults leads the robot to an unwanted pose or even cause singularity.

For the position regulation of CMM, by setting r to be longer than the radius of the robot's physical workspace, the interaction proxy can have the full priority to control the robot in order to take a long-distance movement.

C. Velocity regulation: We set a fuzzy-based velocity boundary for FMM to be

$$B_{v2} = (b_{u2} - b_{l2})\mu_{v2}^{\sigma_2} + b_{l2} \quad (6)$$

where b_{u2} and b_{l2} are two positive constants standing for a large upper bound and a small lower bound. $\sigma_2 > 1$ represents the change rate. μ_{v2} is a fuzzy membership defined as

$$\mu_{v2} = \mu_{1,t_{k-1}} \cdot \mu_{1,t_k} \quad (7)$$

The fuzzy membership μ_{v2} is a multiplication of μ_1 in the current step time and that in the last step time. From (7), $\mu_v = 1$ means the robot is conducting small movement in a certain period ($t_k - t_{k-1}$), so its velocity is not degraded. Once the interaction proxy is moved outside the small workspace during the period, B_{v2} is reduced in order to decrease the velocity. The slower motion of the robot provides more time for the operator to regulate the pose of the interaction proxy.

Note that the MR reference position in CMM is more like a step signal that can introduce position discontinuity. Since the interaction proxy can be freely placed in the physical workspace of the robot, the step reference position can be very large. Therefore, the velocity boundary B_{v1} in CMM should be small at the beginning of the movement, then gradually regulate itself during the movement. Accordingly, the velocity boundary B_{v1} is defined as

$$B_{v1} = \frac{-(b_{u1} - b_{l1})|\mu_{v1} - \frac{1}{2}|^{\sigma_1}}{|\frac{1}{2}|^{\sigma_1}} + b_{u1} \quad (8)$$

where b_{u1} , and b_{l1} are the upper bound and lower bound, and μ_{v1} and σ_1 are defined as

$$\mu_{v1} = \frac{\|X_s - X_o\|_2}{\|e_p\|_2} \quad (9)$$

$$\sigma_1 = (\sigma_u - \sigma_l) * \mu_{v1} + \sigma_l \quad (10)$$

where $\sigma_u > 1$ and $\sigma_l < 1$ are positive constants.

The logic of (8)-(10) is that when the robot is at its initial position, the fuzzy membership μ_{v1} is close to zero that makes the boundary B_{v1} to be its lower bound. Also, the change rate σ_1 is low at the beginning of motion in order to avoid the sudden jump of the robot. During a long-distance movement, the velocity boundary increases to its upper bound in order to accelerate the robot. The change rate σ_1 also becomes high enough to allow the robot to have a fast speed during movement. When the robot is close to its desired pose, μ_{v1} reaches 1 to slow down the motion by lowering the velocity boundary. The trajectory of B_{v1} is a bell-shaped curve. This allows the robot to stably track the interaction proxy.

D. force regulation: In practical industrial applications, normally, the industrial robot is not used to conduct hard contact motion since its large applied force is likely to destroy the environment or itself. However, during the MR-based teleoperation, no matter in CMM or FMM, it is possible that the robot hit some rigid environment due to operational faults. Although the proposed position and velocity regulation strategies can prevent the sudden movement of the robot, the hard contact between the robot and the environment object may still destabilize the overall system or fail tasks.

To prevent the robot from repetitively hitting the environment due to the wrong pose given from the interaction proxy, we design an effective strategy to regulate the robot's force. The estimated external force F_e^* is set to be limited by a

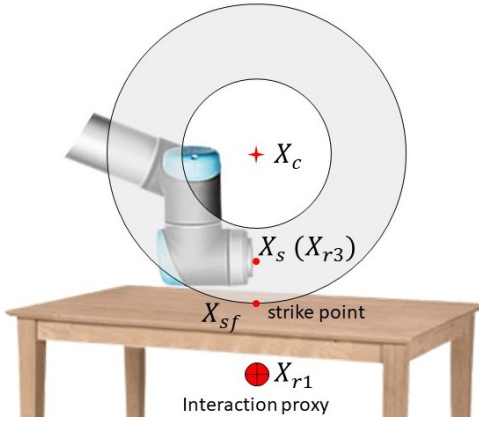


Figure 5. Changing the center of the workspace due to hard contact

constant boundary B_f , and the force exceeding B_f is deemed a hard contact that may make the system crash. If the robot hits a physical barrier when moving to the place set by the interaction proxy, the estimated force will jump close to B_f , and the position of the robot at this moment is recorded as X_{sf} . Then, the feedback force pushes the robot away from the physical barrier like a spring. With the recorded position X_{sf} and the current robot's position X_s , as the example shown in Fig. 5, the center X_c of the concentric circles with radius r and R can be automatically updated. (The created concentric circle in Fig. 5 after contacting to a physical barrier has the same values of r and R as that of the concentric circle in FMM.) That is, by using X_{sf} and X_s to build a straight line, X_c is in this line that satisfy $\|X_{sf} - X_c\|_2 = R$ and $\|X_s - X_c\|_2 \leq \|X_{sf} - X_c\|_2$.

In Fig. 5, based on (2)-(5), the interaction proxy X_{r1} is outside the large circle which means it cannot control the robot to hit the physical barrier again. the robot's current position X_s (X_{r3}) takes the control priority so that the robot will stay at its current position until the operator correctly regulates the interaction proxy's position. This method can prevent the robot getting stuck into hard contact or hitting the physical barrier multiple times due to the spring-like force feedback.

IV. CONTROLLER DESIGN UNDER STATE CONSTRAINTS USING BACK-STEPPING

According to Section 2, the goals of control architecture setup are as follows: 1. The robot can smoothly track the interaction proxy without any perturbations. 2. The internal states of the robot (e.g. velocity, force) have their adaptive boundaries. 3. The system's stability cannot be affected by potential dynamical disturbances. To reach the above goals, this section utilizes the back stepping method to establish the final control laws.

The unknown dynamics of the robot consisting multiple DoF can be expressed as

$$\mathbf{M}_s(q_s)\ddot{q}_s + \mathbf{C}_s(q_s, \dot{q}_s)\dot{q}_s + \mathbf{G}_s(q_s) + \mathbf{B}_s(q_s, \dot{q}_s) = \tau_s + J^T F_e \quad (11)$$

where q_s, \dot{q}_s , and \ddot{q}_s are the vectors of joint displacement, velocity and acceleration. $\mathbf{M}_s(q_s)$ and $\mathbf{C}_s(q_s, \dot{q}_s)$ denote the inertia matrix, and centrifugal and coriolis matrices, respectively.

$\mathbf{G}_s(q_s)$ denotes the gravity and $\mathbf{B}_s(q_s, \dot{q}_s)$ denotes bounded disturbances including robot frictions. $\mathbf{M}_s(q_s)$, $\mathbf{C}_s(q_s, \dot{q}_s)$, $\mathbf{G}_s(q_s)$, and $\mathbf{B}_s(q_s, \dot{q}_s)$ are unknown. τ_s is the control torque. J is the Jacobian matrix that satisfies $\dot{x}_s = J\dot{q}_s$. Therefore, $\ddot{x}_s = J\ddot{q}_s + \dot{J}\dot{q}_s$. F_e is the passive environment force. In this paper, we assume F_e is unknown and we use force observation method in [29] to derive the estimated force F_e^* , which may contain estimation errors as $F_e = F_e^* + \Delta_e$, where Δ_e is the estimation error that consists of unknown dynamics, noises and acceleration information.

Since the above robot dynamics are unknown, we apply the Type-2 fuzzy neural network in [15], [30] to estimate the overall dynamics which attains high accuracy and is robust against uncertainties. Therefore, the dynamics (11) is expressed by a combination of multiple linear local models as

$$M_s\ddot{q}_s + C_s\dot{q}_s + D_sq_s + E_s + \varpi_s = \tau_s + J^T F_e^* \quad (12)$$

where M_s , C_s , D_s and E_s are weighted sums of the local models' coefficients with fuzzy membership grades as weights. The fuzzy membership grads are a group of dynamic functions of the system inputs. ϖ_s is the sum of unknown estimation errors, noises, disturbances and Δ_e . Therefore, M_s , C_s , D_s and E_s are time varying coefficients to describe the nonlinear robotic systems in (11).

The sliding surface of sliding mode control has a significant influence on the robotic system. With the sliding surface converging to zero in a finite time, the desired system performance can be achieved. In this study, the Nonsingular Fast Terminal Sliding Mode (NTFSM) is chosen as

$$s_1 = \int (c_1 \text{sig}^{\varphi_1}(e_s) + c_2 S(e_s) + c_3 \dot{e}_s) \quad (13)$$

where $\text{sig}^a(x) = [|x_1|^{a_1} \text{sign}(x_1), \dots, |x_n|^{a_n} \text{sign}(x_n)]^T$. c_1 , c_2 and c_3 are positive constant control gains. $\varphi_1 > 1$ is a constant, and to avoid singularity, $S(e_s)$ is designed as

$$S(e_s) = \begin{cases} \text{sig}^{\varphi_2}(e_s) & \text{if } e_s \geq \epsilon_s \\ \text{sig}^2(e_s) & \text{if } e_s < \epsilon_s \end{cases} \quad (14)$$

where $0 < \varphi_2 < 1$ is a positive constant and $0 < \epsilon_s \ll 1$ is a small value close to zero.

When the sliding surface in (13) converge to zero, The convergence time can be derived as

$$T_s = \int_0^{|e_s(0)|} \frac{1}{\frac{c_1}{c_3} e_s^{\varphi_1} + \frac{c_2}{c_3} e_s^{\varphi_2}} de_s \leq \frac{c_3}{c_1} \frac{1}{\varphi_1 - 1} + \frac{c_3}{c_1} \frac{1}{1 - \varphi_2} \quad (15)$$

From (15), the small value of c_3 ($c_3 < c_1, c_3 < c_2$) can efficiently shorten the convergence time. The first and the second derivative of the sliding surface s_1 can be written as

$$\begin{aligned} \dot{s}_1 &= c_1 \text{sig}^{\varphi_1}(e_s) + c_2 S(e_s) + c_3 \dot{e}_s \\ \ddot{s}_1 &= c_1 \varphi_1 |e_s|^{\varphi_1-1} \dot{e}_s + c_2 \varphi_2 |e_s|^{\varphi_2-1} \dot{e}_s + c_3 \ddot{e}_s \end{aligned} \quad (16)$$

Substituting the fuzzy-based dynamic model in (12) into (16), and let $\Psi(e_s, \dot{e}_s) = c_1\varphi_1|e_s|^{\varphi_1-1}\dot{e}_s + c_2\varphi_2|e_s|^{\varphi_2-1}\dot{e}_s$, we can derive

$$\begin{aligned}\dot{s}_1 &= s_2 \\ \dot{s}_2 &= s_3 \\ \dot{s}_3 &= \frac{d}{dt}(\Psi(e_s, \dot{e}_s) + c_3(JM_s^{-1}\tau_s + JM_s^{-1}J^TF_e^* - \Omega(q_s, \dot{q}_s) \\ &\quad - \Delta_1 + \dot{J}\dot{q}_s - \ddot{X}_r(t-T)))\end{aligned}\quad (17)$$

where $\Omega(q_s, \dot{q}_s) = JM_s^{-1}C_s\dot{q}_s + JM_s^{-1}D_sq_s + JM_s^{-1}E_s$ are known terms and $\Delta_1 = JM_s^{-1}\varpi_s$ contains unknown noises, disturbances and the errors of environmental force estimation.

To find a proper control input of the robot system in (17) and to simultaneously satisfy the proposed regulations of position, velocity and force introduced in Section 2, a back-stepping design procedure is proposed. The BLF defined in [31] is also applied in the back-stepping design in order to deal with the state constraints. Based on (17), the following change of coordinates is introduced:

$$z_1 = s_1 - \alpha_1, z_2 = s_2, z_3 = s_3 - \alpha_2 \quad (18)$$

where α_1 and α_2 are virtual control terms. Eq. (18) can derive

$$\dot{z}_1 = z_2 - \dot{\alpha}_1 \quad (19)$$

$$\dot{z}_2 = z_3 + \alpha_2 \quad (20)$$

Step 1: Define a positive Lyapunov function V_1 to be

$$V_1 = \frac{1}{2}z_1^T z_1 \quad (21)$$

Choose the virtual control term α_1 to be

$$\dot{\alpha}_1 = k_1 z_1 \quad (22)$$

where k_1 is a positive constant gain. By using (19) and (22), the differential of \dot{V}_1 to be

$$\dot{V}_1 = -k_1 z_1^T z_1 + z_1^T z_2 \quad (23)$$

Step 2: The estimated environmental force is required not to exceed the constant bound B_f , which is defined to be hard contact. Accordingly, the stiffness of the environmental force that corresponds to the robot's position is the main information needed. For simplicity of controller design, We use (24) as a simple expression of F_e^* .

$$F_e^* = -B_e s_2 \quad (24)$$

where B_e is a diagonal matrix that denotes the stiffness of the estimated environmental force. The differential of F_e^* can be expressed as $\dot{F}_e^* = -B_e \dot{s}_2$. Involving the estimated environmental force into BLF, we consider the following Lyapunov function (25) with the condition of $|F_e^*(i)| < B_f(i)$ for future controller design:

$$V_2 = V_1 + \frac{1}{2} \sum_{i=1}^6 \log \frac{B_f(i)^2}{B_f(i)^2 - F_e^*(i)^2} \quad (25)$$

Based on (20)-(24), the differential of V_2 can be derived as

$$\begin{aligned}\dot{V}_2 &= -k_1 z_1^T z_1 + z_1^T z_2 + \sum_{i=1}^6 \frac{B_e(i, i)^2 z_2(i) \dot{z}_2(i)}{B_f(i)^2 - F_e^*(i)^2} \\ &= -k_1 z_1^T z_1 + z_1^T z_2 + z_2^T H z_3 + z_2^T H \alpha_2\end{aligned}\quad (26)$$

where $H = \text{diag}([\frac{B_e(1,1)^2}{B_f(1)^2 - F_e^*(1)^2}, \dots, \frac{B_e(6,6)^2}{B_f(6)^2 - F_e^*(6)^2}])$. By defining the virtual control term to be $\alpha_2 = -H^{-1}z_1 + \alpha_3$, where α_3 is to be introduced later, \dot{V}_2 can be simplified as

$$\dot{V}_2 = -k_1 z_1^T z_1 + z_2^T H z_3 + z_2^T H \alpha_3 \quad (27)$$

Step 3: The robot velocity \dot{X}_s needs to satisfy $B_v > \dot{X}_s$, where $B_v = B_{v1}$ or $B_v = B_{v2}$ is a varying constraint. Based on (16) and (18), $B_v > \dot{X}_s$ can also be rewritten as $\beta_v > z_2$, where β_v is defined as

$$\begin{aligned}\beta_v &= c_1\varphi_1|e_s|^{\varphi_1-1}(B_v - \dot{X}_r(t-T)) \\ &\quad + c_2\varphi_2|e_s|^{\varphi_2-1}(B_v - \dot{X}_r(t-T)) + c_3\ddot{e}_s\end{aligned}\quad (28)$$

Considering the velocity constraint, the following Lyapunov function is applied:

$$V_3 = V_2 + \frac{1}{2} \sum_{i=1}^6 \log \frac{\beta_v(i)^2}{\beta_v(i)^2 - z_3(i)^2} \quad (29)$$

Setting $\eta_s = z_3/\beta_v$, the differential of V_3 is derived as

$$\begin{aligned}\dot{V}_3 &= \dot{V}_2 + \sum_{i=1}^6 \frac{1}{1 - \eta_s^2(i)} \cdot \left(\frac{z_2(i) \dot{z}_2(i)}{\beta_v^2(i)} - \frac{\dot{\beta}_s(i) z_2^2(i)}{\beta_v^3(i)} \right) \\ &= -k_1 z_1^T z_1 + z_2^T H z_3 + z_2^T H \alpha_3 + z_3^T \theta \dot{z}_3 + z_3^T \lambda z_3\end{aligned}\quad (30)$$

where $\theta = \text{diag}([\frac{1}{(1-\eta_s^2(1))\beta_v^2(1)}, \dots, \frac{1}{(1-\eta_s^2(6))\beta_v^2(6)}])$ and $\lambda = \text{diag}([\frac{-\dot{\beta}_s(1)}{(1-\eta_s^2(1))\beta_v^3(1)}, \dots, \frac{-\dot{\beta}_s(6)}{(1-\eta_s^2(6))\beta_v^3(6)}])$. According to (17), by substituting the robot's dynamics into (30), \dot{V}_3 can be further express as

$$\begin{aligned}\dot{V}_3 &= -k_1 z_1^T z_1 + z_2^T H z_3 + z_2^T H \alpha_3 + z_3^T \lambda z_3 \\ &\quad + z_3^T \theta \left(\frac{d}{dt}(\Psi(e_s, \dot{e}_s) + c_3(JM_s^{-1}\tau_s + JM_s^{-1}J^TF_e^* \right. \\ &\quad \left. - \Omega(q_s, \dot{q}_s) - \Delta_1 + \dot{J}\dot{q}_s - \ddot{X}_r(t-T))) - \dot{\alpha}_2 \right)\end{aligned}\quad (31)$$

Setting the control input τ_s to be $\tau_s = \tau_1 + \tau_2 + \tau_3$, and τ_1 and τ_2 are

$$\begin{aligned}\tau_1 &= J^{-1}M_s(\Omega(q_s, \dot{q}_s) - \dot{J}\dot{q}_s + \ddot{X}_r(t-T) + \hat{\Delta}_1) - J^TF_e^* \\ \tau_2 &= -J^{-1}M_s c_3^{-1} \Psi(e_s, \dot{e}_s)\end{aligned}\quad (32)$$

where $\hat{\Delta}_1$ is a uncertainty estimator used to compensate for the side-effect of Δ_1 . By setting $\alpha_3 = -k_2\theta^{-1}H^{-1}z_2$, where k_2 is positive constant gains, the virtual control term α_2 can finally be written as

$$\alpha_2 = -H^{-1}z_1 - k_2\theta^{-1}H^{-1}z_2 \quad (33)$$

Substitute (32)-(33) into (31). With Δ_1 being compensated for, the \dot{V}_3 can be simplified as

$$\begin{aligned}\dot{V}_3 &\leq -k_1 z_1^T z_1 - z_2^T (\theta^{-1}k_2 - \frac{H}{2}) z_2 \\ &\quad + z_3^T \theta \left(\frac{d}{dt}(c_3 JM_s^{-1}\tau_3 - \alpha_2) + \theta^{-1}\lambda z_3 + \frac{1}{2}\theta^{-1}H z_3 \right)\end{aligned}\quad (34)$$

We set τ_3 to be

$$\tau_3 = J^{-1}M_s\left(\frac{\alpha_2}{c_3} - c_3^{-1} \int k_3 z_3\right) \quad (35)$$

where k_3 is a positive gain. Under the situation that the uncertainties are compensated for, \dot{V}_3 can be finally written as

$$\dot{V}_3 \leq -k_1 z_1^T z_1 - z_2^T \left(\theta^{-1} k_2 - \frac{H}{2}\right) z_2 - z_3^T (\theta k_3 - \lambda - H) z_3 \quad (36)$$

where $\theta^{-1} k_2 \geq \frac{H}{2}$ and $\theta k_3 \geq \lambda + \frac{H}{2}$. Then, \dot{V}_3 is negative semidefinite, which implies that the terms z_1, z_2, z_3 will converge to zero in a finite time. Therefore, it can be concluded that the proposed back-stepping NTFSM system is asymptotically stable.

To design the uncertainty estimator, the fuzzy-based system dynamics in (12) can be re-arranged as

$$\begin{cases} \dot{\kappa}_1 = \kappa_2 \\ \dot{\kappa}_2 = JM_s^{-1}\tau_s + JM_s^{-1}J^T F_e^* - \Omega(q, \dot{q}) + \dot{J}\dot{q}_s - \kappa_3 \\ \dot{\kappa}_3 = \omega \end{cases} \quad (37)$$

where $\kappa_1 = X_s$, $\kappa_2 = \dot{X}_s$ and $\kappa_3 = \Delta_1$ are the states in (37), ω is the differential of the unknown uncertainty.

Based on the dynamic state function in (37), we propose the uncertainty estimator as

$$\begin{cases} \dot{Y}_1 = Y_2 - d_1 \varepsilon_1 \\ \dot{Y}_2 = JM_s^{-1}\tau_s + JM_s^{-1}J^T F_e^* - \Omega(q, \dot{q}) + \dot{J}\dot{q}_s - Y_3 \\ \quad - d_2 \varepsilon_2 - d_3 \varepsilon_1 \\ \dot{Y}_3 = -d_4 \text{sig}^{\varphi_2}(\varepsilon_1) \end{cases} \quad (38)$$

where d_{1-4} are constant parameters. ε_{1-3} are defined as

$$\varepsilon_1 = Y_1 - \kappa_1, \varepsilon_2 = Y_2 - \kappa_2, \varepsilon_3 = Y_3 - \kappa_3 \quad (39)$$

From (37) and (38), we derive

$$\begin{cases} \dot{\varepsilon}_1 = \varepsilon_2 - d_1 \varepsilon_1 \\ \dot{\varepsilon}_2 = -\varepsilon_3 - d_2 \varepsilon_2 - d_3 \varepsilon_1 \\ \dot{\varepsilon}_3 = -d_4 \text{sig}^{\varphi_2}(\varepsilon_1) - \omega \end{cases} \quad (40)$$

During the steady state with $\dot{\varepsilon}_{1,2,3} = 0$, the state function in (40) can be expressed as

$$\begin{cases} |\varepsilon_2| = d_1 \left| \frac{\omega}{d_4} \right|^{\frac{1}{\varphi_2}} \\ |\varepsilon_3| = d_2 d_1 \left| \frac{\omega}{d_4} \right|^{\frac{1}{\varphi_2}} + d_3 \left| \frac{\omega}{d_4} \right|^{\frac{1}{\varphi_2}} \\ |\varepsilon_1| = \left| \frac{\omega}{d_4} \right|^{\frac{1}{\varphi_2}} \end{cases} \quad (41)$$

From (41), by selecting d_4 to be large enough and with $\frac{1}{\varphi_2}$ that can make $\left| \frac{\omega}{d_4} \right|$ small enough, ε_1 can be efficiently guaranteed to be small, which makes ε_2 and ε_3 to be close to zero at the steady state. Therefore, with Y_1 and Y_2 closely tracking to κ_1 and κ_2 , Y_3 can be guaranteed to track the uncertainties. In (32), $\hat{\Delta}_1$ is the output Y_3 of (38).

For the control law $\tau = \tau_1 + \tau_2 + \tau_3$, τ_1 is used to strengthen the system stability by compensating for the system dynamics and uncertainties. τ_2 is actually a velocity damper related to the position errors. At the steady state with the position error e_s close to zero or the velocity error \dot{e}_s close to zero, τ_2 is close to zero. In τ_3 , based on (20), (22), and (33), α_2 can be written to be

$$\alpha_2 = -H^{-1} \frac{k_1}{\mathbb{S} + k_1} \frac{s_2}{k_1} - k_2 \theta^{-1} H^{-1} s_2 \quad (42)$$

\mathbb{S} denotes the Laplace operator. $\frac{k_1}{\mathbb{S} + k_1}$ can be seen as a low-pass filter with its cut-off frequency k_1 . During free motion ($F_e^* = 0$), where $\max(H^{-1})$ is $\text{diag}(\frac{B_f(1)^2}{B_e(1,1)^2}, \dots, \frac{B_f(6)^2}{B_e(6,6)^2})$.

Substituting (42) into (35), we can see that during free motion, θ^{-1} can regulate the velocity according to the changing velocity constraints B_{v1} and B_{v2} . when contacting a physical barrier, the term H^{-1} can make τ_3 decrease to zero. By virtue of the spring-like feedback force provided by $-J^T F_e^*$ in τ_1 , the robot will leave the physical barrier. Meanwhile, the sphere workspace is changed so that the interaction proxy loses its control priority and the robot can stay at its current position rather than hit the physical barrier again.

V. DISCUSSION

This paper introduces a new MR-based teleoperation system for telepresence and maneuverability enhancement, which has the main contributions on the following three aspects.

1). For telepresence enhancement of the system design, a novel MR-based interface is designed that makes an effective combination between virtual and real components. From the designed MR interface, the 3D model of the robot which dynamically follows the real robot's state and the point cloud from the camera provides the operator with the full sight about the movement of the robot and the remote environment, which allows to clearly grasp the situation of the environment and the robot's work performance. Previous research has already demonstrated superiority of VR-based interfaces over conventional displays. For instance, in [32], the authors demonstrate significant improvement of collaborative task performance when users are provided with stereoscopic vision feedback. Further, a quantitative evaluation of improvement of a VR-based interface is provided in [28], which provides better situational awareness through HMD pose tracking on a teleoperation task. In our system, the interface implements a AV paradigm, in which a virtual scene is augmented by the real-time data from the robot's task space. The choice of using an AV-based interface is stipulated by several factors. Firstly, similar to previous MR-based interfaces, in the current study, the operators can freely move in the space and view the task space from different angles. The stereoscopic vision and parallax are achieved by using a HMD and head-pose tracking. The interaction of operators with virtual objects in the scene is done by using hand-gesture tracking. Secondly, to decouple the operator from the control loop and thus eliminate some control noise, the operator can only interact with virtual objects and their gestures are not directly tracked by the robot. Finally, a AV-based interface offers better opportunities for incorporating visual cues for the operator, such as using spot

lights in the task space, which opens up possibilities to isolate operators from distractors and direct attention into the task.

2). For maneuverability enhancement of the system design, a new interaction proxy is proposed for human-machine interaction that makes a large improvement compared to the systems proposed in [22], [27], [28], [33]. In these systems, the operator uses the physical handles to directly control the robot, and cannot let go of the handles when performing the tasks. This control mode has three main drawbacks: First, it compels the robot to always track the human behaviour. Subsequently, the operator should be very cautious and cannot freely move during the whole control process, and sometimes s/he has to keep a uncomfortable gesture to drive the robot for a long time, which make the teleoperation become a physically and mentally exhausting job. Second, with the physical restrictions of the master controllers [27], it suffers workspace difference and kinematic redundancy between the master and the slave so that the workspace of the slave robot can be seriously restricted and pose of the robot cannot be fully used. Third, it has no fault tolerance on the human motion. The inevitable body shaking of the operator can cause chattering of the robot that may fail the overall task. Therefore, these systems are not very user-friendly and do not support long-time human operation. On the contrary, the proposed interaction proxy allows the operator to be freely decoupled from the control loop. It does not require the operator to hold anything, and offers the operator a large degree of freedom that s/he can conduct the teleoperation in a comfortable human motion without worrying about his/her unintentional movement damaging the robot or failing the task. Also, the operator can freely manage the breaking time when performing a task that s/he can stop to take a rest or to observe the robot's states and motion in order to better plan the next step in teleoperation. Besides, the interaction proxy has no physical limitations such that it can take full advantage of the robot's overall workspace and pose. Moreover, this interaction proxy provides virtual buttons for the operator to freely use in order to implement different functions of the robot (e.g. "activate/deactivate button").

3). Based on the authors' best knowledge, most of the existing VR-based teleoperation systems do not consider the robot state regulation, which is closely related to the system maneuverability and the task achievement (e.g. [22], [24], [25], [28], [33]). On the control algorithms design of this paper, two control modes, CMM and FMM, are proposed for both coarse movement and fine movement of the robot. In the two control modes, different state regulation strategies are designed to improve the robot's movement. the effective combination of these two control modes has the following advantages. First, CMM can decouple the proxy out of the control loop and allow the operator to freely regulate the desired position and orientation of the robot without influencing the robot. In FMM, the operator only needs to control the position rather than exhaustively pays attention to both position and orientation of the robot. Second, when doing fine works, the untrained operator may move the interaction proxy to a wrong place which will mislead the robot or damage the environment. The proposed fuzzy-based position regulation method in (1)-(5) has strong tolerance on such this fault of operation that restricts

the robot's motion in a online-updating small workspace. Third, the velocity regulation strategy in (6)-(10) effectively deals with the motion discontinuity problem caused by the discontinuous reference position from the interaction proxy that offers the robot smooth and safe motions with adaptive velocity. Forth, without haptic feedback, the operator cannot control the contact force to the environment of the previous system [22] which can seriously threaten the safety. In the proposed system, the force restriction strategy enables the robot to always gently contact to the environment however large the interaction proxy's movement is. This strategy can guarantee the system's safety during contact.

VI. EXPERIMENTAL RESULTS

In this section, experimental results are presented to demonstrate the effectiveness of the proposed MR-based teleoperation system. The overall experimental setup includes a Universal Robot (UR10) mounted with a Robotiq-85 industrial gripper, an RGB-D sensor (Asus Xtion Pro), and a HTC Vive MR helmet mounted with a Leap Motion hand gesture sensor. ROS is used on the slave side as a foundation for the robot's control algorithms. The time delay between the interface side and the UR10 robot is around 200 ms. The control gains of the proposed control algorithm are set to be $B_e = 0.1$, $\varphi_1 = 2$, $\varphi_2 = 0.8$, $k_1 = 20$, $k_2 = 40$, $k_3 = 20$, $d_1 = 2.8$, $d_2 = 11$, $d_3 = 4.5$, $d_4 = 7.5$. The gains for the sliding surface s_1 are set as $c_1 = 0.5$, $c_2 = 0.5$, $C_3 = 0.1$.

A. CMM test

In the first experiment, we test the position and velocity regulation in CMM in Fig. 6. In this experiment, the UR10 robot conducts a relatively long-distance movement. The lower boundary b_{l1} and upper boundary b_{u1} of the velocity are set to be 0.1 m/s and 0.4 m/s. The upper and lower bound of the change rate σ_1 is set to be $\sigma_u = 6$ and $\sigma_l = 0.5$. In CMM, the radius of the concentric sphere workspace R and r are larger than the robot's physical workspace ($R = 2.1$ m, $r = 2$ m), so the interaction proxy has full control of the robot. Fig. 7 shows the position and orientation tracking between the robot and the interaction proxy, and Fig. 8 shows velocity regulation of the robot during a long-distance movement. In the two figures, at the 4.2 s, the pose of the interaction proxy has a sudden change. Then, since the velocity boundary is at its lower bound, the robot starts moving at a low velocity. During the movement, the boundary change rate increases from 0.5 to 6 that makes the the velocity boundary gradually increase to its upper bound 0.4 m/s. Thus, the robot can have a relatively high speed during the movement. When reaching the desired pose, the velocity boundary automatically decreases to 0.1 m/s in order to allow the robot to have a stable tracking to the desired pose. During the overall movement, by using BLF, the robot's velocity can be efficiently limited by the variable velocity boundary; and the proposed sliding surface can provide the robot a fast and stable tracking performance.

In comparison, previous studies (e.g. [22], [28], [33]) always couple the robot motion with the operators' movement and gesture, in which the operator has to physically grasp a handle

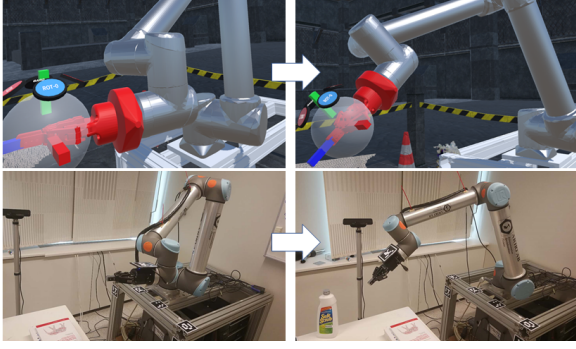


Figure 6. Experiment for CMM

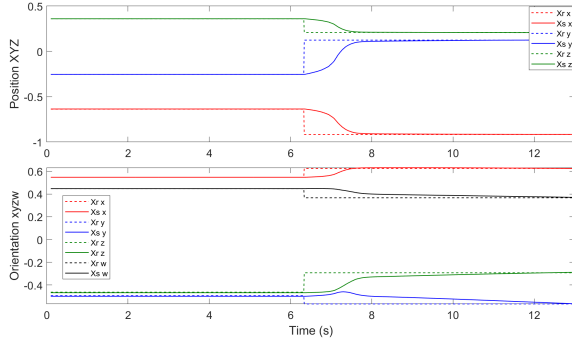


Figure 7. Position and orientation tracking in CMM

and cannot let go of it when controlling the robot. The inevitable body shaking of the operator can cause chattering of the robot that may fail the overall task, and the operator has an uncomfortable pose to control the robot.

B. FMM test

In the second experiment, we test the position and velocity regulation in FMM as shown in Fig. 9. FMM is used to provide the robot continuous tracking in some fine movements. Fig.

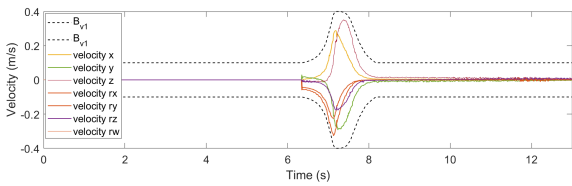


Figure 8. Velocity regulation in CMM



Figure 9. Experiment for FMM

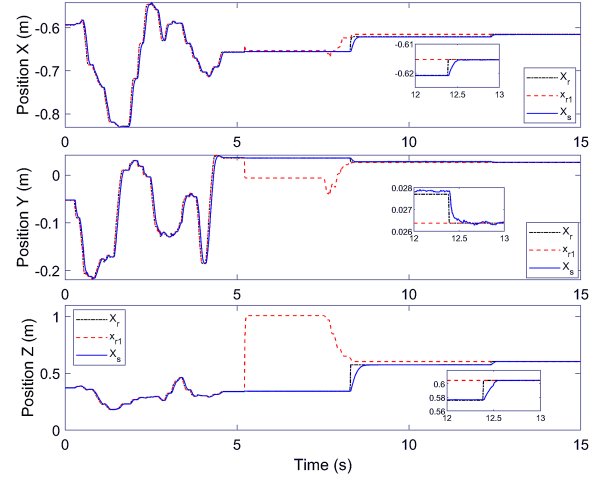
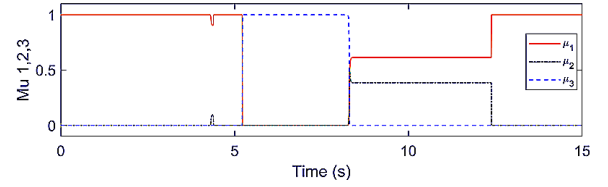


Figure 10. Position regulation in FMM

Figure 11. μ_1 , μ_2 , and μ_3

10 shows the position regulation, Fig. 11 shows the fuzzy memberships and Fig. 12 shows the velocity regulation. The upper and the lower velocity boundaries are $b_{u2} = 0.8$ m/s and $b_{l2} = 0.3$ m/s. The radius of the concentric sphere workspaces are $r = 0.2$ m and $R = 0.3$ m, respectively. The change rates σ and ι for the fuzzy membership in (2) are set to be 4 and 200. During FMM, the robot's orientation is constant as it is pre-determined by that in CMM. In these figures, before 5 s, the interaction proxy is moved within the small sphere workspace, so that it has the full control of the robot. Also, since the velocity boundary is not decreased (μ_1 is always 1), the robot can have a fast and close tracking to the interaction proxy. In addition, the workspace keeps updating so that the robot position does not have a strict limitation. At the 5.3 s, the operator makes an operational fault in which the interaction proxy is suddenly pushed faraway as shown in Fig. 9. μ_3 immediately changes to 1 that makes the robot stay at its current position rather than follow the interaction proxy. The fuzzy-based position regulation can efficiently prevent the robot from reaching unwanted pose which may have a potential danger of failing tasks. The velocity boundary also

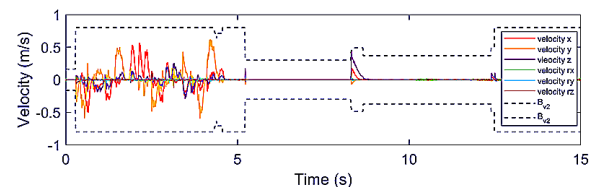


Figure 12. Velocity regulation in FMM

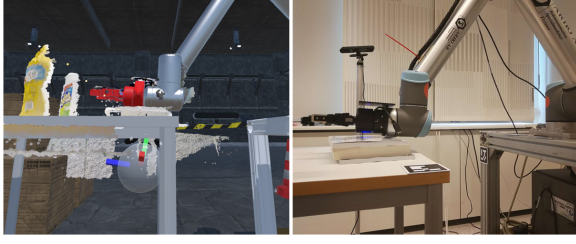


Figure 13. Experiment for force regulation

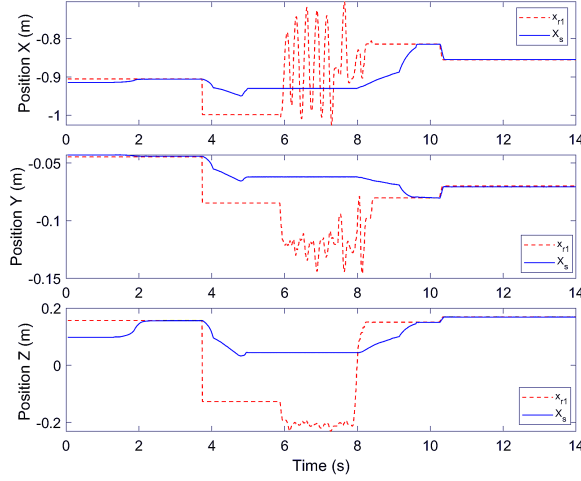


Figure 14. position under contact

decreases to 0.3 m/s. When moving the interaction proxy to a reasonable position, the robot is gradually close to the interaction proxy and finally tracks to the interaction proxy. Note that from 8 s to 13 s, the robot tracks to X_r , rather than the interaction proxy. Then, we set a timer on this situation. When the interaction proxy is not moved any more and the pre-defined time reaches, the robot will finally tracks to the interaction proxy. This is used to give the operator enough time to adjust the interaction proxy to a desired pose. From 5.3 s to 13 s, the velocity is bounded to be low because of the operational fault which can prevent the robot from suddenly jumping to a worse pose. After the robot tracks interaction proxy in a reasonable pose, the velocity boundary can be automatically restored.

In comparison, in [22], [28], [33], since the robot always tracks operator's physical handle, if such systems repeat our experiment by fast moving their handle far away from the robot, the robot will track the handle to a wrong place in an uncontrollable speed that will threaten the system's safety.

C. Force regulation test

In this experiment, we test the force regulation of the control system as shown in Fig. 13. The force boundary B_f is set to be 1N. Fig. 14 and Fig. 15 show the position and the environmental force under the contact motion. From 3.8 s, the robot follows the position of the interaction proxy to move down and at 5 s, the robot contacts to a physical barrier (a pile of books). At this sudden time, the environmental force is close to the boundary B_f that makes τ_3 close to zero. Therefore,

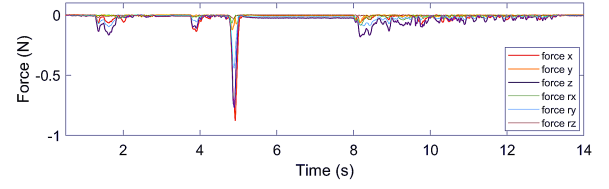


Figure 15. force under contact

the feedback force $-J^T F_e^*$ makes the robot jump up a little to leave the physical barrier. Also, the workspace is changed accordingly. Therefore, even the interaction proxy is largely moved under the pile of books from 6 s to 8 s, the robot will not follow the interaction proxy to contact the physical barrier again. When the interaction proxy is moved above the pile of books (moved into the workspace), the robot will track the interaction proxy again. The UR10 robot is very sensitive to the environmental force and may apply a very large force that can potentially damage environmental objects, fail the task or cause dangers. This method can restrict the force and prevent the robot from hitting the physical barrier again.

Without any force control method, [22], [28], [33] will punch rather than gently touch the environment that will damage the robot and the system will crash.

D. Comparison using pick-and-place experiments

Fig. 16 shows an example of pick-and-place experiment using the proposed system. The operator firstly uses CMM to regulate the orientation of the UR10 robot in order to better grasp the task object (the yellow bottle) in the next moves (Fig. 16.1 - Fig. 16.2). Then, FMM is applied to move the robot's end effector to grasp and lift the object (Fig. 16.3). In the next step, the yellow bottle is accurately and stably placed at the top of the white bottle (Fig. 16.4). According to the proposed force control, when the yellow bottle contacts to the white one, the feedback force prevents the gripper from keeping pressing. Hence, the yellow bottle is gently placed rather than "squeezing" the white one. After the gripper looses the object, the operator uses CMM to move the robot back to its original position and orientation (Fig. 16.5 - Fig. 16.6).

A series of experiments repeating the above pick-and-place experiment in Fig. 16 are conducted to make a quantitative comparison between our proposed system and the traditional system in [28]. In the system of [28], the position and orientation of the robot are fully controlled by a tool physically handled by the operator without force control algorithms. Each of the two systems conducts the above pick-and-place experiment for 16 trials.

We define that a successful trial must satisfy the following three conditions.

- 1). Orientation change is requested. The robot's tool is parallel to the table at origin and must point down to grasp the bottle as Fig. 16.1 - 16.3.
- 2). The yellow bottle must be placed onto the white one and both of them must not fall down as Fig. 16.5 - Fig. 16.6.
- 3). During contact, the robot must not crash. (The ur10 robot is extremely sensitive to the environmental force. Large contact force can easily make the overall system crash.)

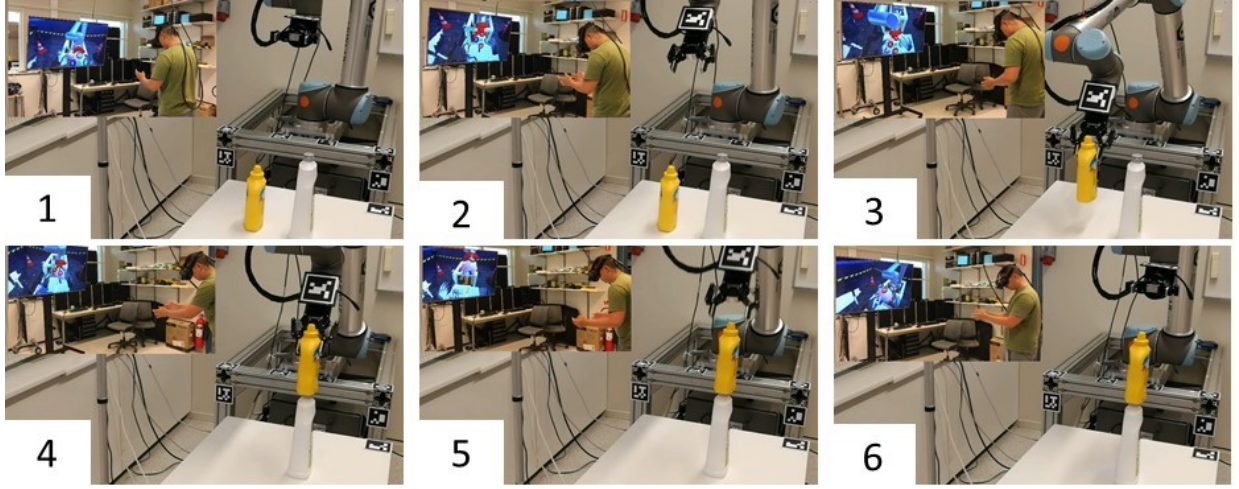


Figure 16. Real pick-and-place experiment. The yellow bottle is gently placed above the white bottle by using the proposed MR-based teleoperation system.

The overall results of the 32 trials are shown in Table I and Table II. In these two tables, we use five subjects to evaluate the performances of the two systems. "Failure 1" denotes that the bottles fall down. "Failure 2" denotes that the system crashes due to the large contact force when putting the yellow bottle onto the white one. " F_e^* at Z" denotes the estimated environmental force at Z axis when the robot places the yellow bottle to the white one. Also, Since F_e^* more than 2.5N can easily make the system crash, F_e^* at Z axis must satisfy $F_e^* < 2.5N$. "Time" denotes the operation time for performing a pick-and-place task (from Fig. 16.1 to Fig. 16.6.). (For the failed trials, the operation time denotes the period from beginning to the time at which the failures occur.) "S?" denotes if the experiment is successful.

Table I
COMPARISON EXPERIMENTS USING THE TRADITIONAL SYSTEM

| Num | Failure 1 | Failure 2 | F_e^* at Z | Time | S? |
|-----|-----------|-----------|--------------|------|-----|
| 1 | Yes | No | 0N | 117s | No |
| 2 | Yes | No | 0N | 97s | No |
| 3 | Yes | No | 1.57N | 132s | No |
| 4 | No | Yes | 3.64N | 91s | No |
| 5 | Yes | No | 0.53N | 93s | No |
| 6 | No | No | 2.02N | 147s | Yes |
| 7 | Yes | No | 0N | 81s | No |
| 8 | Yes | No | 1.32N | 105s | No |
| 9 | No | Yes | 4.85N | 118s | No |
| 10 | No | No | 1.5N | 104s | Yes |
| 11 | Yes | No | 2.03N | 124s | No |
| 12 | No | No | 2.21N | 159s | Yes |
| 13 | No | Yes | 5.78N | 92s | No |
| 14 | No | Yes | 3.31N | 136s | No |
| 15 | Yes | No | 0N | 101s | No |
| 16 | No | No | 1.76N | 88s | Yes |

By comparing the results in the two tables, the success rate of our system (15/16) is much larger than that of the traditional system (4/16), which is led by the following reasons. First, the operators using the traditional system need to simultaneously take care of both position and orientation of the robot and the robot's speed does not have adaptive regulation. As a result, a operator needs to be very skillful to drive the robot and any humanly shaking may cause "Failure 1" (the bottles

Table II
COMPARISON EXPERIMENTS USING OUR SYSTEM

| Num | Failure 1 | Failure 2 | F_e^* at Z | Time | S? |
|-----|-----------|-----------|--------------|------|-----|
| 1 | No | No | 0.84N | 73s | Yes |
| 2 | Yes | No | 0N | 91s | No |
| 3 | No | No | 0.21N | 134s | Yes |
| 4 | No | No | 0.93N | 84s | Yes |
| 5 | No | No | 0.53N | 72s | Yes |
| 6 | No | No | 0.64N | 97s | Yes |
| 7 | No | No | 0.59N | 69s | Yes |
| 8 | No | No | 0.22N | 81s | Yes |
| 9 | No | No | 0.86N | 85s | Yes |
| 10 | No | No | 0.92N | 77s | Yes |
| 11 | No | No | 0.78N | 95s | Yes |
| 12 | No | No | 0.80N | 120s | Yes |
| 13 | No | No | 0.12N | 79s | Yes |
| 14 | No | No | 0.70N | 98s | Yes |
| 15 | No | No | 0.29N | 75s | Yes |
| 16 | No | No | 0.82N | 78s | Yes |

fall down). Besides, as the operators have to keep a specified posture and cannot be decoupled from the control loop during manipulation, it is difficult to clearly check the task's status (e.g. check whether the yellow bottle contacts to the white one when the robot is placing the bottle). Therefore, the robot can easily drop the bottle rather than place the bottle as shown by the trails with 0N in " F_e^* at Z" in Table I. In comparison, the operators using our system can switch control modes to regulate the robot's pose and is freely to be decoupled from the control loop to check the task's status. Therefore, the object becomes easier to be picked and placed using our system. Second, the traditional system without force control is likely to punch the object with large force that causes "Failure 2". The operators have to be very careful to guide the robot otherwise the overall system will crash. The trials in Table I with force larger than 2.5N cause "Failure 2". In comparison, as shown in Table II, with the proposed force control, the robot in our system can gently place the object and the forces are lower than the force boundary (1N) in all trails. The average operation time of the 15 successful trails using our system is 87.8s which is lower than that of the 4 successful trails

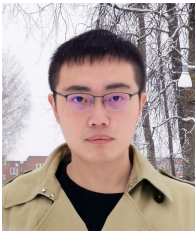
using the traditional system 124.5s. The higher success rate and the lower operation time demonstrate that our system is more effective and user-friendly than its counterpart.

VII. CONCLUSIONS

In this paper, a new MR-based teleoperation system is proposed to provide an immersive visual feedback to the operator. In the proposed MR-based teleoperation, two control modes are designed to improve the long-distance movement and fine movement of the robot. A series of fuzzy-based methods are also proposed to regulate the position, velocity, and force of the robot in order to improve the system maneuverability. Control laws based on BLF and the backstepping control procedure can guarantee the system stability under state constraints. With the immersive visual feedback and regulated system states, the telepresence of the overall system can be enhanced, which potentially leads to the reduced operational workload, and the increased task success rate. Multiple experimental results have been done to show the feasibility of the proposed system.

REFERENCES

- [1] Peter F Hokayem and Mark W Spong. Bilateral teleoperation: An historical survey. *Automatica*, 42(12):2035–2057, 2006.
- [2] Farzad Hashemzadeh, Mojtaba Sharifi, and Mahdi Tavakoli. Nonlinear trilateral teleoperation stability analysis subjected to time-varying delays. *Control Engineering Practice*, 56:123–135, 2016.
- [3] Harun Tugal, Joaquin Carrasco, Pablo Falcon, and Antonio Barreiro. Stability analysis of bilateral teleoperation with bounded and monotone environments via zames–falb multipliers. *IEEE Transactions on Control Systems Technology*, 25(4):1331–1344, 2017.
- [4] R Baranitha, R Rakkiyappan, Reza Mohajerpour, and Saba Al-Wais. Stability analysis of nonlinear telerobotic systems with time-varying communication channel delays using general integral inequalities. *Information Sciences*, 2018.
- [5] Da Sun, Qianfang Liao, and Hongliang Ren. Type-2 fuzzy logic based time-delayed shared control in online-switching tele-operated and autonomous systems. *Robotics and Autonomous Systems*, 101:138–152, 2018.
- [6] Amit Milstein, Tzvi Ganel, Sigal Berman, and Ilana Nisky. Human-centered transparency of grasping via a robot-assisted minimally invasive surgery system. *IEEE Transactions on Human-Machine Systems*, (99), 2018.
- [7] Farhad Azimifar, Saman Ahmadvosrabi Rozi, Ahmad Saleh, and Iman Afyouni. Transparency performance improvement for multi-master multi-slave teleoperation systems with external force estimation. *Transactions of the Institute of Measurement and Control*, page 0142331217740178, 2017.
- [8] Da Sun, Fazel Naghdy, and Haiping Du. Transparent four-channel bilateral control architecture using modified wave variable controllers under time delays. *Robotica*, 34(4):859–875, 2016.
- [9] Da Sun, Fazel Naghdy, and Haiping Du. Time domain passivity control of time-delayed bilateral telerobotics with prescribed performance. *Nonlinear dynamics*, 87(2):1253–1270, 2017.
- [10] Allison M Okamura. Methods for haptic feedback in teleoperated robot-assisted surgery. *Industrial Robot: An International Journal*, 31(6):499–508, 2004.
- [11] Zhenyu Lu, Panfeng Huang, and Zhengxiong Liu. Predictive approach for sensorless bimanual teleoperation under random time delays with adaptive fuzzy control. *IEEE Transactions on Industrial Electronics*, 65(3):2439–2448, 2017.
- [12] Keyvan Hashtrudi-Zaad and Septimiu E Salcudean. Transparency in time-delayed systems and the effect of local force feedback for transparent teleoperation. *IEEE Transactions on Robotics and Automation*, 18(1):108–114, 2002.
- [13] Murat Cenk Çavuşoğlu, David Feygin, and Frank Tendick. A critical study of the mechanical and electrical properties of the phantom haptic interface and improvements for highperformance control. *Presence: Teleoperators & Virtual Environments*, 11(6):555–568, 2002.
- [14] Costas Tzafestas, Spyros Velanas, and George Fakiridis. Adaptive impedance control in haptic teleoperation to improve transparency under time-delay. In *Robotics and Automation, 2008. ICRA 2008. IEEE International Conference on*, pages 212–219. IEEE, 2008.
- [15] Da Sun, Qianfang Liao, Xiaoyi Gu, Changsheng Li, and Hongliang Ren. Multilateral teleoperation with new cooperative structure based on reconfigurable robots and type-2 fuzzy logic. *IEEE transactions on cybernetics*, 49(8):2845–2859, 2018.
- [16] Linping Chan, Fazel Naghdy, and David Stirling. Position and force tracking for non-linear haptic telemanipulator under varying delays with an improved extended active observer. *Robotics and Autonomous Systems*, 75:145–160, 2016.
- [17] Zhenyu Lu, Panfeng Huang, Zhengxiong Liu, and Haifei Chen. Fuzzy observer-based hybrid force/position control design for a multiple-sampling-rate bimanual teleoperation system. *IEEE Transactions on Fuzzy Systems*, 2018.
- [18] Verena Nitsch and Berthold Farber. A meta-analysis of the effects of haptic interfaces on task performance with teleoperation systems. *IEEE transactions on haptics*, page 1, 2012.
- [19] Panfeng Huang, Pei Dai, Zhenyu Lu, and Zhengxiong Liu. Asymmetric wave variable compensation method in dual-master-dual-slave multilateral teleoperation system. *Mechatronics*, 49:1–10, 2018.
- [20] Ken Goldberg, Michael Mascha, Steve Gentner, Nick Rothenberg, Carl Sutter, and Jeff Wiegley. Desktop teleoperation via the world wide web. In *Robotics and Automation, 1995. Proceedings., 1995 IEEE International Conference on*, volume 1, pages 654–659. IEEE, 1995.
- [21] Paul Milgram, Haruo Takemura, Akira Utsumi, and Fumio Kishino. Augmented reality: A class of displays on the reality-virtuality continuum. In *Telemanipulator and telepresence technologies*, volume 2351, pages 282–293. International Society for Optics and Photonics, 1995.
- [22] Filippo Brizzi, Lorenzo Peppoloni, Alessandro Graziano, Erika Di Stefano, Carlo Alberto Avizzano, and Emanuele Ruffaldi. Effects of augmented reality on the performance of teleoperated industrial assembly tasks in a robotic embodiment. *IEEE Transactions on Human-Machine Systems*, 2018.
- [23] Holly A Yanco, Jill L Drury, and Jean Scholtz. Beyond usability evaluation: Analysis of human-robot interaction at a major robotics competition. *Human-Computer Interaction*, 19(1):117–149, 2004.
- [24] Curtis W Nielsen, Michael A Goodrich, and Robert W Ricks. Ecological interfaces for improving mobile robot teleoperation. *IEEE Transactions on Robotics*, 23(5):927–941, 2007.
- [25] Henrique Martins and Rodrigo Ventura. Immersive 3-d teleoperation of a search and rescue robot using a head-mounted display. In *Emerging Technologies & Factory Automation, 2009. ETFA 2009. IEEE Conference on*, pages 1–8. IEEE, 2009.
- [26] Firas Abi-Farraj, Claudio Pacchierotti, Oleg Arenz, Gerhard Neumann, and Paolo Robuffo Giordano. A haptic shared-control architecture for guided multi-target robotic grasping. *IEEE transactions on haptics*, 2019.
- [27] Dejing Ni, AYC Nee, SK Ong, Huijun Li, Chengcheng Zhu, and Aiguo Song. Point cloud augmented virtual reality environment with haptic constraints for teleoperation. *Transactions of the Institute of Measurement and Control*, page 0142331217739953, 2018.
- [28] David Whitney, Eric Rosen, Elizabeth Phillips, George Konidakis, and Stefanie Tellex. Comparing robot grasping teleoperation across desktop and virtual reality with ros reality. In *Proceedings of the International Symposium on Robotics Research*, 2017.
- [29] Da Sun, Qianfang Liao, Todor Stoyanov, Andrey Kiselev, and Amy Loutfi. Bilateral telerobotic system using type-2 fuzzy neural network based moving horizon estimation force observer for enhancement of environmental force compliance and human perception. *Automatica*, 106:358–373, 2019.
- [30] Qian-Fang Liao and Da Sun. Interaction measures for control configuration selection based on interval type-2 takagi–sugeno fuzzy model. *IEEE Transactions on Fuzzy Systems*, 26(5):2510–2523, 2018.
- [31] Beibei Ren, Shuzhi Sam Ge, Keng Peng Tee, and Tong Heng Lee. Adaptive neural control for output feedback nonlinear systems using a barrier lyapunov function. *IEEE Transactions on Neural Networks*, 21(8):1339–1345, 2010.
- [32] O. Liu, D. Rakita, B. Mutlu, and M. Gleicher. Understanding human-robot interaction in virtual reality. In *2017 26th IEEE International Symposium on Robot and Human Interactive Communication (RO-MAN)*, pages 751–757, Aug 2017.
- [33] Jeffrey I Lipton, Aidan J Fay, and Daniela Rus. Baxter’s homunculus: Virtual reality spaces for teleoperation in manufacturing. *IEEE Robotics and Automation Letters*, 3(1):179–186, 2018.



Da Sun received the B.Eng. and Ph.D. degrees in mechatronics from the University of Wollongong, Wollongong, NSW, Australia, in 2012 and 2016, respectively. From 2016 to 2017, he was a Research Fellow with the National University of Singapore, Singapore. He is currently a researcher at the Center for Applied Autonomous Sensor Systems (AASS) at Örebro University, Örebro, Sweden. His research interests include robotics learning, modelling, and control theory.



Andrey Kiselev is a researcher at the Center for Applied Autonomous Sensor Systems (AASS) at Örebro University, Sweden. He received his Engineer degree in Computer Systems from the Moscow Institute of Electronic Technology in 2004 and PhD degree in Informatics from Kyoto University in 2011 in the field of human-computer interaction. His current research interests are in Human-Robot Interaction, Robotic Telepresence, and Teleoperation.



Qianfang Liao received the B.Eng. degree in automation from Wuhan University, Wuhan, China, in 2006, the M.Eng. degree in automation from Shanghai Jiao Tong University, Shanghai, China, in 2009, and the Ph.D. degree from the School of Electrical and Electronic Engineering, Nanyang Technological University, Singapore, in 2015. Currently, she is a researcher with Örebro University, Örebro, Sweden. Her research interests include fuzzy modeling, control theory, and computer vision.



Todor Stoyanov is an associate professor (docent) with the Center for Applied Autonomous Sensor Systems, Örebro University, Sweden. He received a Master's degree in Smart Systems from Jacobs University Bremen in 2008 and a Ph.D. degree in computer science from Örebro University, Sweden, in 2012. His main interests include 3D mapping and localization, 3D perception, and mobile manipulation. Major contributions over the past five years include: map building and range data fusion, grasp planning and grasp execution control, as well as

learning for manipulation.



Amy Loutfi is a professor in Information Technology at Örebro University with the Center for Applied Autonomous Sensor Systems (AASS), Sweden. Her general interests are in the area of integration of artificial intelligence with autonomous systems, and over the years has looked into applications where robots closely interact with humans in both industry and domestic environments. She received her Ph.D in Computer Science in 2006 with her thesis focussed on the integration of artificial olfaction on robotic and intelligent systems to enable good

human-robot interaction. Since then, she has examined various cases of human robot interaction including applications of telepresence.